The Hindmarsh–Rose neuron model: Bifurcation analysis and piecewise-linear approximations

Marco Storace,[1,a)] Daniele Linaro,[1] and Enno de Lange[2,b)]
[1]*Department of Biophysical and Electronic Engineering, University of Genoa, Via Opera Pia 11a, I-16145 Genova, Italy*
[2]*Laboratory of Nonlinear Systems, School of Computer and Communication Sciences, École Polytechnique Fédérale de Lausanne, Lausanne, Switzerland*

(Received 6 May 2008; accepted 28 July 2008; published online 5 September 2008)

This paper provides a global picture of the bifurcation scenario of the Hindmarsh–Rose model. A combination between simulations and numerical continuations is used to unfold the complex bifurcation structure. The bifurcation analysis is carried out by varying two bifurcation parameters and evidence is given that the structure that is found is universal and appears for all combinations of bifurcation parameters. The information about the organizing principles and bifurcation diagrams are then used to compare the dynamics of the model with that of a piecewise-linear approximation, customized for circuit implementation. A good match between the dynamical behaviors of the models is found. These results can be used both to design a circuit implementation of the Hindmarsh–Rose model mimicking the diversity of neural response and as guidelines to predict the behavior of the model as well as its circuit implementation as a function of parameters. © *2008 American Institute of Physics*. [DOI: 10.1063/1.2975967]

The fundamental building block of every nervous system is the neuron. There is an increasing trend towards studying the behavior of relatively large networks (e.g., millions) of neurons and modeling/emulating such networks. To do that, a significant common effort is necessary, which involves several disciplines, such as biology, neuroscience, physics, mathematics, computer science, and electronics. One of the main reasons of this trend is strictly connected with the research effort in understanding how the brain works. In this kind of research activity, it is necessary to combine experimental studies of animal and human nervous systems with numerical simulation of mathematical models. From a biophysical-mathematical point of view, to model the electrical behavior of a biological neuron is one of the main problems. In developing such models, a compromise must be found between two seemingly mutually exclusive requirements: the model for a single neuron must be computationally simple and, at the same time, capable of mimicking almost all the behaviors exhibited by real biological neurons (in particular the rich firing patterns). Understanding the dynamics of single neurons and their role within larger neural networks is therefore at the core of neuroscience. There exists biologically plausible models that allow one to simulate large size neuron networks. Brain function, however, relies on the interplay of hundreds to billions of neurons that are arranged in specialized modules on multiple anatomical hierarchies. Up to now, the simulation of large networks of single- or multicompartment neural models is still unrealistic if not hardware implemented. On the other hand, the actual circuit implementations of neurons exhibit behaviors only partially similar to those of the corresponding models. The aim of this paper is twofold. The first is a two-parameter bifurcation analysis of the Hindmarsh–Rose model, carried out by combining simulations with continuation methods. Also the influence of two further bifurcation parameters on the model dynamics is investigated. The analysis provides a global bifurcation scenario where the bifurcation curves are organized by codimension-two bifurcation points. The scenario outlining the organizing structure of the model can be used in modeling studies, for instance to facilitate the choice of a region of search and initial values for parameter fitting. The second aim is to apply a recently proposed method (based on piecewise-linear approximations) for the circuit implementations of ordinary differential equations (ODEs) to the Hindmarsh–Rose model. Also, the approximate models are analyzed and the comparisons with the bifurcation scenario of the Hindmarsh–Rose model exhibit good matchings. The approximate models will correspond to circuits with two control parameters, allowing one to obtain rather different spike-train patterns as responses to identical input currents, i.e., diversity of the neural response.

I. INTRODUCTION

The phenomenological neuron model proposed by Hindmarsh and Rose (HR) (Refs. 1 and 2) may be seen either as a generalization of the Fitzhugh equations[3] or as a simplification of the physiologically realistic model proposed by Hodgkin and Huxley.[4] It has proven to be a single-compartment model providing a good compromise between two seemingly mutually exclusive requirements: The model for a single neuron must be both computationally simple, and

[a)]Electronic mail: marco.storace@unige.it.
[b)]Present address: Department of Physiology, University of Bern, Bern, Switzerland.

capable of mimicking almost all the behaviors exhibited by real biological neurons (in particular the rich firing patterns).[5]

Real neurons show a variety of dynamical behaviors, according to the values of biophysical parameters.[6] Among the most important ones, one may find (for examples, see Fig. 8, gray lines):

- *Quiescence*: the input to the neuron is below a certain threshold and the output reaches a stationary regime.
- *Spiking*: the output is made up of a regular series of equally spaced spikes.
- *Bursting*: the output is made up of groups of two or more spikes (called bursts) separated by periods of inactivity.
- *Irregular spiking*: the output is made up of an aperiodic series of spikes.
- *Irregular bursting*: the output is made up of an aperiodic series of bursts.

The HR model is able to reproduce all these dynamical behaviors and has been analyzed in the past, with respect to one or two bifurcation parameters.[7–13] In the bifurcation analysis carried out in the cited references, particular attention has been devoted to study the transitions between stable bursting solutions and continuous spiking regimes and the fold of cycles bifurcations cascade leading, through a period-adding mechanism, to the transitions between quiescent asymptotic behaviors and bursting regimes. The first goal of this paper is to provide a global picture of the bifurcation scenario with respect to two parameters (i.e., the input current and the other parameter of the fast subsystem, controlling the transition between spiking and bursting), with an insight to the effects of two further parameters. The bifurcation scenario is analyzed by combining simulations with continuation methods, showing that the bifurcation curves are organized by few codimension-two bifurcation points. We used the continuation packages MATCONT (Ref. 14) and AUTO2000 (Ref. 15) for the continuation of equilibria and limit cycles and of their codimension-one bifurcations. More in particular, we used the package HOMCONT (Ref. 16) (included in AUTO2000) to continue homoclinic bifurcations and detect their codimension-two degeneracies.[17] The combined method of analysis we use is very general and can be applied to a large class of continuous-time smooth dynamical systems.[18] The global bifurcation scenario provides concrete information about the HR model, that may be useful in more biophysically oriented studies, for instance, in modeling studies as a guide to choose the parameters for fitting the model to qualitatively different types of electrophysiological behaviors.[19,20]

The second goal is to apply to the HR model a method for the circuit synthesis of nonlinear dynamical systems based on the following main tools: a technique for the piecewise-linear (PWL) approximation and circuit synthesis of multivariate nonlinear functions;[21–25] optimization methods, and in particular genetic algorithms;[26] bifurcation analysis through numerical methods, using both simulations and continuation techniques.[27,28] In particular, the focus of the second part of the paper will be on finding a reliable PWL approximation of the HR model. To check the reliability of the PWL approximations, a two-dimensional bifurcation diagram is obtained also for properly smoothed versions of the PWL models. The results show a good matching with respect to the bifurcation diagram of the HR model.

We point out that the main advantages in choosing the HR model are two: (i) its vector field exhibits only two nonlinear (polynomial) terms and (ii) there already exist circuit syntheses,[29,30] where the only control parameter is the bias current. Therefore this model is a good benchmark to test the proposed method, in view of both a circuit implementation of the HR model as a component of a network and, if useful, the application of the whole approximation/synthesis procedure to more complex (and physiologically realistic) neuron models, such as the Hodgkin–Huxley one.[4]

The rest of this contribution is organized as follows: Sec. II briefly introduces the HR model, whose bifurcation analysis with respect to two parameters is carried out in Secs. III and IV. The main PWL approximation results are shown in Sec. V.

II. THE HR MODEL

The HR model[2] is able to reproduce all the dynamical behaviors listed in the Introduction and is described by the following set of ODEs:

$$\dot{x} = y - x^3 + bx^2 + I - z,$$

$$\dot{y} = 1 - 5x^2 - y, \tag{1}$$

$$\dot{z} = \mu[s(x - x_{\text{rest}}) - z].$$

Roughly, the roles played by the system parameters are the following: I mimics the membrane input current for biological neurons; b allows one to switch between bursting and spiking behaviors and to control the spiking frequency; μ controls the speed of variation of the slow variable z in Eq. (1) (i.e., the efficiency of the slow channels in exchanging ions) and, in the presence of spiking behaviors, it governs the spiking frequency, whereas in the case of bursting, it affects the number of spikes per burst; s governs adaptation: a unitary value of s determines spiking behavior without accommodation and subthreshold adaptation, whereas values around $s=4$ give strong accommodation and subthreshold overshoot, or even oscillations; x_{rest} sets the resting potential of the system.

In the following, we will present a bifurcation analysis of the HR model with respect to b, I and, to a lesser extent, μ and s. The remaining parameter is $x_{\text{rest}}=-1.6$.

III. BRUTE-FORCE BIFURCATION ANALYSIS

In this section we propose the first bifurcation analysis results, i.e., a description of the overall bifurcation scenario and the results of a brute-force bifurcation analysis, for $\mu=0.01$ and $s=4$.

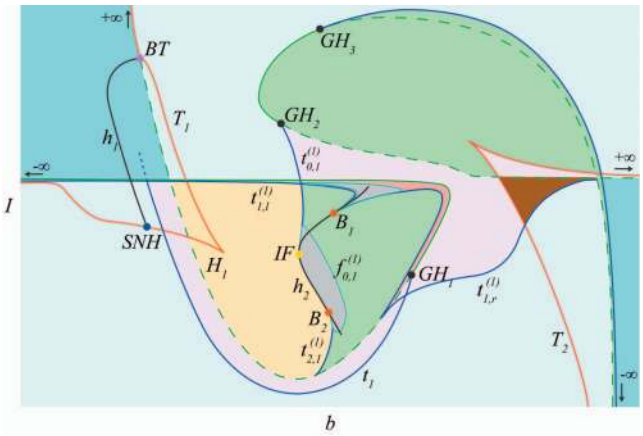

FIG. 1. (Color) Qualitative sketch of the overall bifurcation scenario.

A. Overall bifurcation scenario

A qualitative bifurcation diagram of the HR model is sketched in Fig. 1. The overall bifurcation diagram is roughly divided into eight regions, characterized by qualitatively different asymptotic (stable) behaviors. Some regions have been represented larger than in reality. The meaning of the colors is as follows:

- in the pale cyan region, the HR neuron is quiescent (only one stable equilibrium);
- in the light blue region, the HR neuron is quiescent (two coexisting stable equilibria);
- in the green region, the HR neuron is spiking regularly;
- in the yellow region, the HR neuron is bursting regularly;
- in the pink region, the system admits two coexisting stable invariant sets, i.e., one stable limit cycle (either spiking or bursting) and one stable equilibrium;
- in the pale red region, the system admits two stable "simple" (spiking) limit cycles;
- in the brown region, the system admits three coexisting stable invariant sets, i.e., one stable limit cycle and two stable equilibria;
- in the gray regions, the system admits "nontrivial" periodic and nonperiodic (either stable or unstable) solutions, then periodic and/or nonperiodic solutions (irregular spiking or bursting) can be observed.

Examples of asymptotic trajectories, corresponding to the dots labeled from (a) to (h) in Figs. 2(a), are shown in Fig. 8 (gray lines).

The parameter space is partitioned into the seven regions by the following bifurcation curves: T_1 and T_2 fold of equilibria (red); H_1 and H_2 Hopf (green), either supercritical (solid lines) or subcritical (dashed lines); t_1, $t_{1,l}^{(1)}$, $t_{1,r}^{(1)}$, and $t_{2,1}^{(1)}$ fold of cycles (blue); $f_{0,1}^{(1)}$ period doubling (cyan); h_1 and h_2 homoclinic (black). We conjecture that the fold curve t_1 ends on a codimension-two point on the homoclinic curve h_1, but there is no numerical evidence of this fact. In any case, this kind of analysis is of negligible practical interest, since in reality the curves t_1 and H_1 are almost overlapping.

B. Brute-force bifurcation diagram

The brute-force bifurcation diagram shown in Fig. 2(a) has been obtained by means of extensive simulations [numerical integrations of system (1)]. As a first step, a regular grid of points has been defined in the parameter plane (b,I). Then, we have defined the Poincaré section $y-x^3+bx^2+I-z=0$, that corresponds to the maxima of x. For each pair of parameter values belonging to the grid, after having discarded the transient evolution, at most 200 consecutive one-directional intersections of each trajectory with the Poincaré section have been recorded looking for periodicity in the evolution of the system. The classification is based on the number of different values of z corresponding to these intersection points. In synthesis, when the z value is unique, the neuron is spiking, whereas multiple values of z may correspond to either bursting or chaotic (i.e., irregular) behaviors. In the absence of periodicity, the behavior has been classified as "chaotic." The quiescence is checked during the transient evolution. Eventually, the bifurcation diagram has been obtained by associating a different color to different asymptotic dynamical behaviors of the system. The diagram points out that the HR model exhibits all the above mentioned dynamical behaviors: cyan represents quiescence, green is for spiking, yellow is for bursting, and black is for chaos. Moreover, yellow changes to red as the number of spikes per burst increases, while green tends to become darker as the spiking frequency increases.

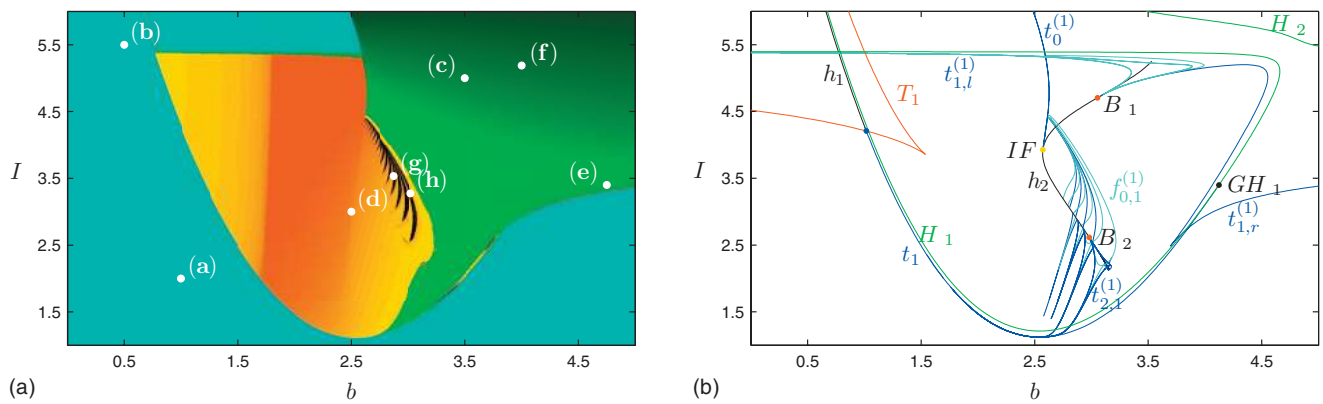

FIG. 2. (Color) (a) Brute-force bifurcation diagram. (b) Continuation analysis bifurcation diagram.

The presence of regions admitting coexisting asymptotic behaviors cannot be directly inferred from the colors.

IV. CONTINUATION ANALYSIS AND SPECIFIC BIFURCATIONS

The (qualitative) borders of the regions described in the previous section are actually induced by (quantitative) bifurcation lines. The invariant sets involved in these bifurcations may be both stable and unstable, or only unstable. In this section, we consider continuation techniques, instead of simulation, to perform bifurcation analysis. Continuation methods allow one to translate the bifurcation analysis of equilibria and cycles into the solution of an implicit algebraic equation which can be computed systematically. Hence, the bifurcation analysis is reduced to locating the zeroes of some functions, which can be found, with the desired precision, by using Newton-based algorithms.

There are several advantages to using continuation methods as opposed to simulation in systems analysis:

- The solutions can be followed in the parameter space even if they are unstable: by contrast, simulation allows the observation of stable solutions only. In this regard, it should be noted that unstable periodic orbits, and in particular saddles, are involved in many bifurcation phenomena. Furthermore, the saddles' invariants separate the basins of attraction of different attractors.
- There is no need to wait for transients to settle before studying the invariants.
- The results are independent of the choice of Poincaré section.
- Numerical problems associated with sensitivity to the initial conditions are avoided.
- Continuation makes it possible to detect hysteretic phenomena due to coexisting attractors. This is difficult to achieve by simulation methods.

The sketch in Fig. 1 has been obtained by reducing and interpreting a thorough bifurcation analysis performed by combining "brute-force" simulations with numerical continuation analysis. The most significant part of the quantitative bifurcation diagram corresponding to the aforesaid sketch is shown in Fig. 2(b).

The details of the different parts making up the bifurcation diagram and its link to the qualitative analysis/partition described in the previous section are discussed in the following. In the scenarios sketched in the next figures, the bifurcating invariant sets are represented according to the following code: stable (unstable) equilibria are represented as dots (crosses), whereas the presence of m stable (unstable) limit cycles is pointed out by the label m^s (m^u).

A. Bifurcations of equilibria

The most external bifurcation lines bordering the simple oscillatory regimes and the coexistence of simple oscillatory solutions are related to bifurcations of equilibria.

The system (1) can have at most three equilibria. The three equilibria exist within the regions bordered by the curves T_1 and T_2, marking fold bifurcations of equilibria. Out of these regions, only one equilibrium (say, E_3) exists. On the curves H_1 and H_2, the equilibrium E_3 undergoes a Hopf bifurcation (either supercritical or subcritical), thus generating a (spiking) limit cycle.

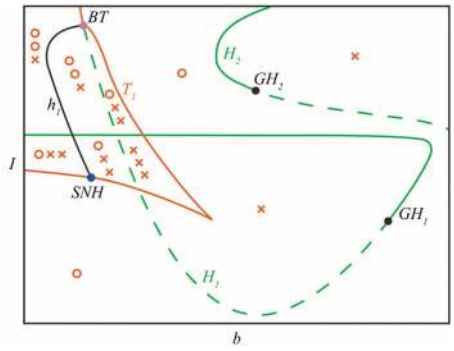

FIG. 3. (Color online) Bifurcation curves for equilibria.

The bifurcation curves for equilibria are sketched in Fig. 3, where only the equilibria are shown.

B. Bogdanov–Takens: Existence of a global bifurcation

At the upper intersection between H_1 and T_1, E_1 and E_2 undergo a Bogdanov–Takens (double zero) bifurcation (point BT in Fig. 1). Hence, in the intersection point BT a global bifurcation curve h_1 is rooted, on which an unstable cycle degenerates, through a taming approach (E_2 is a saddle with real eigenvalues and two-dimensional stable manifold), to a homoclinic orbit to E_2.

Despite the global bifurcation, BT still organizes only simple behaviors, though degeneracies of h_1 are good candidates for justifying other more complex behaviors.

C. Noncentral saddle-node degeneracy

By numerically continuing the homoclinic bifurcation curve h_1 far away from BT, a first *global* degeneracy is detected at the point *SNH* (see Fig. 1), where the homoclinic bifurcation undergoes a *noncentral saddle-node degeneracy*.[17] This codimension-two bifurcation point acts as an organizing center for excitability in many dynamical systems.[31]

D. Generalized-Hopf points

As shown in Fig. 1, both H_1 and H_2 contain generalized-Hopf degeneracies (GH_1 on H_1, GH_2, and GH_3 on H_2), where the numerically calculated first Lyapunov coefficient changes its sign, thus changing the supercritical/subcritical nature of the bifurcation.

The system unfolding around the generalized-Hopf bifurcation points is standard, even at a nonlocal scale.

E. Inclination flip degeneracy

The fold bifurcation of cycles $t_0^{(1)}$ rooted in GH_2 ends in an *inclination flip* degeneracy *IF*,[17,32,33] detected numerically with HOMCONT on h_2. The eigenvalues of E_3 (saddle-node with two-dimensional unstable manifold) at *IF* are approxi-

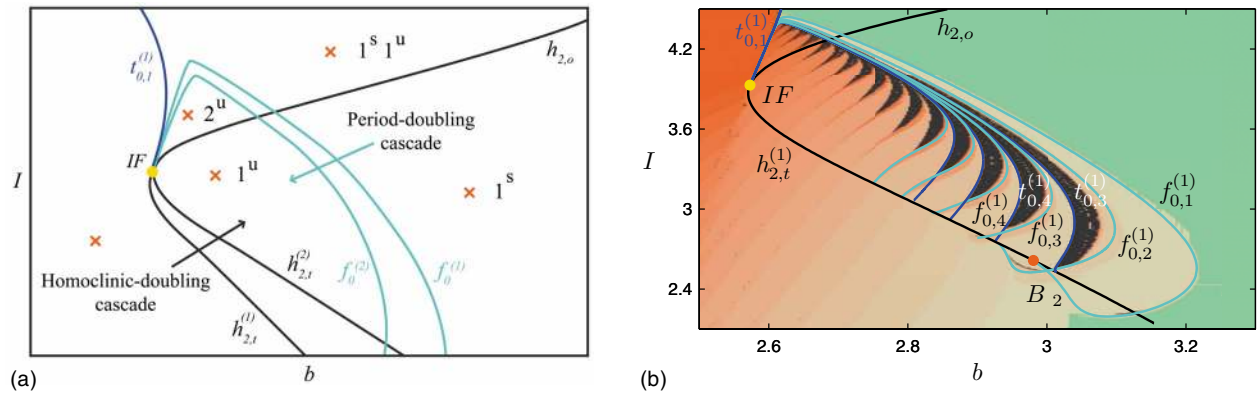

FIG. 4. (Color online) System unfolding around the codimension-two bifurcation point *IF*. (a) Qualitative bifurcation diagram. (b) Corresponding quantitative curves obtained by numerical continuation.

mately −4.5125, 0.3302, and 0.0159. The codimension-two bifurcation point *IF* splits h_2 into two homoclinic bifurcation branches $h_{2,o}$ and $h_{2,t}^{(1)}$, where the homoclinic orbit is oriented and twisted, respectively. Moreover, an infinite series of period-doubling bifurcations and an infinite series of (secondary) homoclinic doubling bifurcation curves are rooted in *IF*, as qualitatively sketched in Fig. 4(a) (only the simplest bifurcating invariant sets are shown). Some of the corresponding quantitative curves obtained by numerical continuation and superimposed to the brute-force bifurcation diagram are shown in Fig. 4(b). The curves of the homoclinic doubling cascade are not distinguishable.

Henceforth, we shall label as $t_{j,k}^{(n)}$ the fold curves originating from the jth codimension-two bifurcation point ($j=0,1,2$ corresponding to *IF*, B_1, and B_2, respectively) located on a homoclinic curve whose originating cycle has n turns. Furthermore, k indicates the number of turns of the cycles colliding on the curve. Analogously, the flip curves have been labeled as $f_{j,k}^{(n)}$. In this case, k indicates the kth flip bifurcation in a Feigenbaum cascade.

The family of homoclinic bifurcations rooting in *IF* organizes the structure of the so-called chaotic region. This region is fractionalized in subregions of chaotic and/or periodic behavior, and the attractors (cycles and strange attractors) are characterized by different geometries, namely, by a different number of oscillations. The series of Feigenbaum-type cascades that exists on the right-hand side of the chaotic region is also organized by the same bifurcation structure. Indeed, the curves $t_{0,k}^{(n+1)}$ and $f_{0,k}^{(n)}$ on the right-hand side of Fig. 4(b) form the skeleton of the series of Feigenbaum's cascades described in Refs. 11 and 12. In fact, the curve $t_{0,k}^{(n+1)}$ is the fold bifurcation that opens the periodic window of period-$(n+1)$, and the curve $f_{0,k}^{(n)}$ is the first flip of the period-$(n+1)$ cycle.

F. Belyakov degeneracies

The homoclinic bifurcation curve $h_{2,o}$ undergoes a Belyakov degeneracy (see the point $B_1^{(1)}$ in Fig. 1), where the equilibrium E_3 changes from saddle (real) to saddle-focus. This degeneracy has been detected numerically with HOMCONT. Theory predicts several families (of infinite cardinality) of bifurcation curves rooting in this point and accumulating exponentially on $h_{2,o}$.[17,34–36] The outer curves delimit a region where wild (chaotic) trajectories can be observed.[37] The quantitative bifurcation curves obtained by numerical continuation are shown in Fig. 5(a).

Actually, the homoclinic bifurcation curve $h_{2,o}$ is U-shaped, but with a very sharp U-turn. For sufficiently low values of both b and I, the right branch of $h_{2,o}$ corresponds to homoclinic orbits to a saddle with a single maximum of x. Going up along the right branch we pass a first Belyakov point $B_1^{(1)}$, and above that point we have homoclinic orbits to a saddle-focus. Proceeding further, after the turning point we encounter a second Belyakov point $B_1^{(2)}$ (in Fig. 5(a) $B_1^{(1)}$ and $B_1^{(2)}$ are indistinguishable), after which we have again homoclinic orbits to a saddle. While making the U-turn, the geometry of the homoclinic orbit changes significantly because a second maximum of x appears; the homoclinic orbit then makes two global turns. The U-turn is very sharp, and the two homoclinic branches, as well as the two Belyakov points, almost coincide in the (b,I)-plane, so that we were unable to resolve them. It is very difficult to numerically produce more than a few of the subsidiary curves that accumulate exponentially on the primary homoclinic curve $h_{2,o}$ and have infinite-order tangency to it at the Belyakov point. In the present case we were able to compute (through continuation) only the first fold of cycles and the first flip bifurcation curves of the corresponding families, as shown in Fig. 5(a). The tangent bifurcation $t_{1,1}^{(1)}$ starts from $B_1^{(1)}$ and, after two cusps, another tangent bifurcation $t_{1,2}^{(1)}$ returns to $B_1^{(2)}$. The flip bifurcation $f_{1,1}^{(1)}$ starts and returns to the same Belyakov point $B_1^{(1)}$.

The same observations can be applied, *mutatis mutandis*, to the homoclinic bifurcation curve $h_{2,t}^{(1)}$, that in turn undergoes a Belyakov degeneracy (see the point $B_2^{(1)}$ in Fig. 1). The bifurcation curves obtained by numerical continuation are shown in Fig. 5(b). The labels GF_1 and GF_2 mark the presence of two generalized-flip points.

G. Orbit flip degeneracies

Any homoclinic bifurcation curve $h_{2,t}^{(k)}$ rooting in *IF* has an orbit flip (or orbit switch) degeneracy $OF^{(k)}$. At this degeneracy point, the homoclinic orbit departs from the saddle

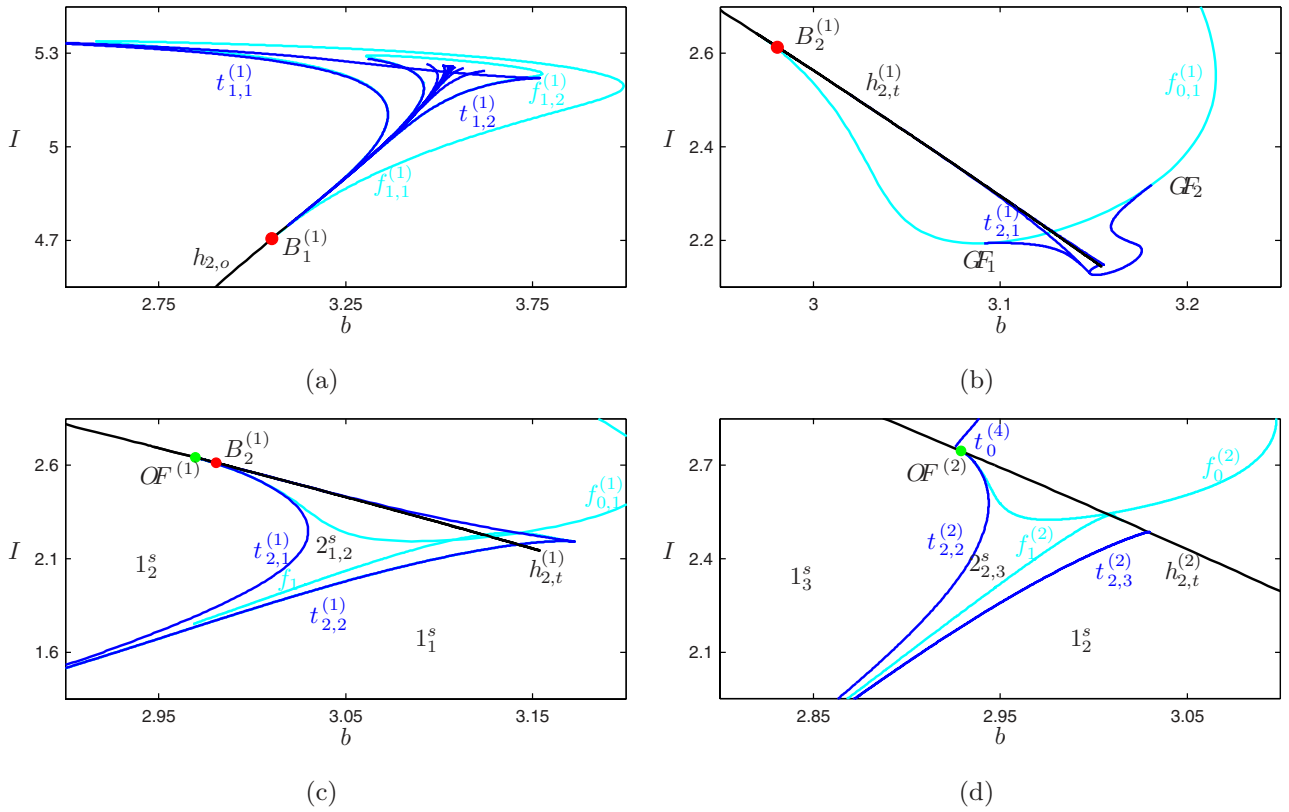

FIG. 5. (Color online) Bifurcation diagrams around the Belyakov points B_1 (a) and B_2 (b), and around the orbit flip degeneracies $OF^{(1)}$ (c) and $OF^{(2)}$ (d). All the curves have been obtained by numerical continuation.

E_3 along its unstable nonleading eigenvector.[17,33,38] Consequently, while crossing $OF^{(k)}$, the departure direction along the unstable leading eigenvector switches.

The unfolding in the parameter space around an orbit flip point depends on the relative arrangement of the saddle eigenvalues.[33] For a relative arrangement of the saddles eigenvalues equivalent to ours, where (in absolute value) the stable eigenvalue is larger than the two unstable ones, the local bifurcation scenario (not completely known) contains a fold of cycles and a flip curve, besides an infinite series of secondary homoclinic bifurcation curves originating at $OF^{(k)}$.[33]

Figure 5(c) shows the arrangement around $OF^{(1)}$ of the bifurcation curves obtained by numerical continuation. The fold of cycles $t^{(1)}_{2,1}$ and the flip curve $f^{(1)}_{0,1}$ are clearly visible even at this scale. The secondary homoclinic bifurcation curves are indistinguishable with respect to $h^{(1)}_{2,t}$. Only the simplest stable bifurcating invariant sets are shown; m stable limit cycles with n_i $(i=1,\ldots,m)$ turns are labeled as $m^s_{n_1,\ldots,n_m}$.

This figure points out the period-adding mechanism leading to bursting behaviors. Below the curve $t^{(1)}_{2,2}$ there is only a stable 1-turn cycle, which collides with an unstable 2-turn cycle on the curve $t^{(1)}_{2,1}$. The unstable cycle, in turn, collides with a stable 2-turn cycle on the curve $t^{(1)}_{2,2}$. Then, between $t^{(1)}_{2,2}$ and $t^{(1)}_{2,1}$ (more precisely, in the subregion above the flip curves $f^{(1)}_{0,1}$ and f_1) there coexist two stable cycles (with one and two turns), whereas above $t^{(1)}_{2,1}$ there is only a stable 2-turn cycle.

Owing to this period-adding mechanism, that replicates for cycles with higher numbers of turns [the local scenario around $OF^{(2)}$ is shown in Fig. 5(d)], we obtain cycles corresponding to bursting behaviors.

H. Bifurcation scenarios in other parameter planes

The bifurcation scenarios of μ as a function of the input current I are extensively studied in Ref. 12 as are, to a lesser extent, the ones with respect to s. An essential point is that the scenario is similar for any nontrivial combination of bifurcation parameters; the razor-shaped area with chaotic lobes observed in Fig. 2 and magnified in Fig. 4(b) can also be identified in the case when μ or s is the second bifurcation parameter, as shown in Fig. 6 (upper panels). Since μ is a parameter of the third (slow) equation, increasing μ from values close to 0 will in essence smear out details in the bifurcation plot of b vs I, as is shown in Fig. 6 (lower panel), where rough brute-force bifurcation diagrams on the parameter plane (b,I) are displayed, together with the Hopf bifurcation curves H_1, for different values of μ. As μ increases, the razor-shaped region becomes larger and has fewer different lobes, until, for values of μ approaching 0.1, no chaos can be observed anymore; similarly, the active region of the model bounded by the Hopf bifurcation curve becomes smaller and smaller, until, for μ just below 0.4 it disappears altogether. A similar compressing behavior can be observed for parameter s, which also modulates the slow equation (see Fig. 6).

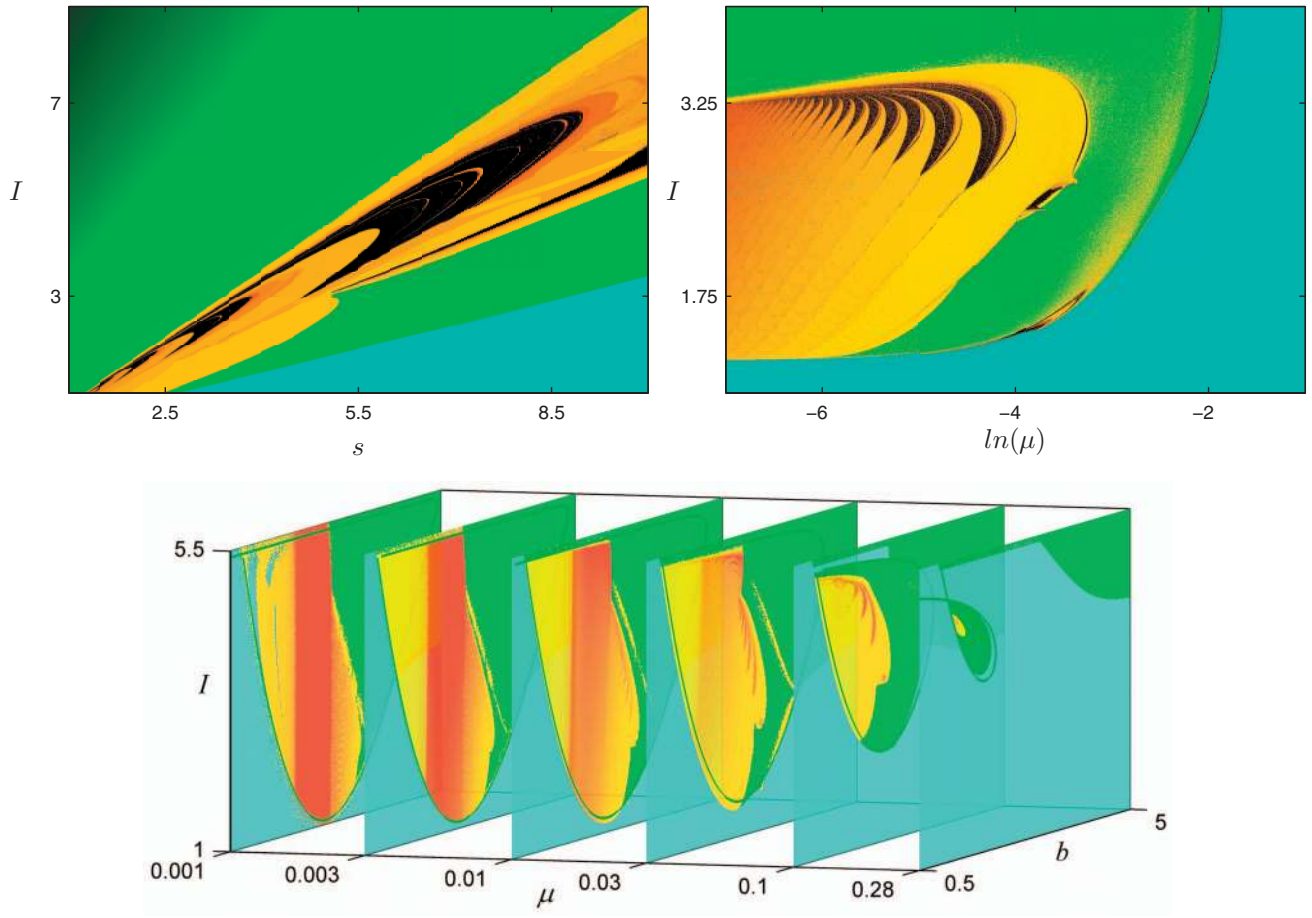

FIG. 6. (Color) Brute-force bifurcation diagrams on the planes (s,I) (upper-left panel) and (μ,I) (upper-right panel, where the μ axis is logarithmically spaced). Influence of μ on the b vs I bifurcation scenario (lower panel).

In the next sections, a PWL approximation of the HR model will be obtained, and the dynamical behaviors of the approximated system will be compared to the original ones.

V. PWL APPROXIMATION OF THE HR MODEL: RESULTS AND DISCUSSION

We provide some basic elements of the PWL approximation method we apply to the HR model. The reader may refer to Refs. 21–23, 27, and 28 for a detailed description of the techniques used here. Many PWL models belong to the class of function expansion models,

$$f_{i\mathrm{PWL}}(\mathbf{y};N)=\sum_{k=1}^{N} w_k^i(N)\varphi_k(\mathbf{y};N), \tag{2}$$

where $f_{i\mathrm{PWL}}$ is a component of the vector of functions $\boldsymbol{f}_{\mathrm{PWL}}$, $\mathbf{y}=(\mathbf{x}^T;\mathbf{p}^T)^T$ is a generic (real) input vector, and N is the (integer) number of basis functions $\varphi_k(\mathbf{y};N)$ whose sum [weighted by the coefficients $w_k^i(N)$] provides an approximation of a given scalar function f_i (which, in our case, is the ith component of the vector field $\boldsymbol{f}$). This is a very broad-spectrum class of models, including, for instance, kernel estimators based on Bayesian methods[39] or on regularization methods,[40] splines[41] and, in the PWL framework, wavelets and prewavelets[42] and fuzzy models.[43]

Since we are interested in implementing the single HR neuron model as an electronic circuit, to be used as a component of a network, we will refer to the technique (*simplicial PWL approach*) proposed in Refs. 21–23, 27, and 28. Generally speaking, a realistic circuit synthesis should be based on a finite set of simple building blocks and, possibly, on (parallel) architectures where identical structures are repeated modularly. The simplified PWL approach satisfies both these requirements.[24,25,44]

In the chosen technique, the PWL functions that approximate the vector field over a given compact domain are based on *a priori* domain partitions through simple type-1 triangulations (or *simplicial partitions*). The simplices (or simplexes) are obtained by subdividing each domain component into a fixed number of identical segments, and each PWL function is affine over each simplex. We remark that a crucial point in the approximation procedure is the choice of the basis functions $\varphi_k(\mathbf{y};N)$ whose weighted sum provides the PWL functions. From a circuit implementation standpoint, the most useful bases are the so-called α-basis, which is suitable for mixed-signal circuit implementations,[44,45] and β-basis, which is suitable for analog circuit implementations.[24]

In the first case, the number of domain subdivisions along each dimensional component is fixed by the circuit architecture. For instance, in the implementations proposed

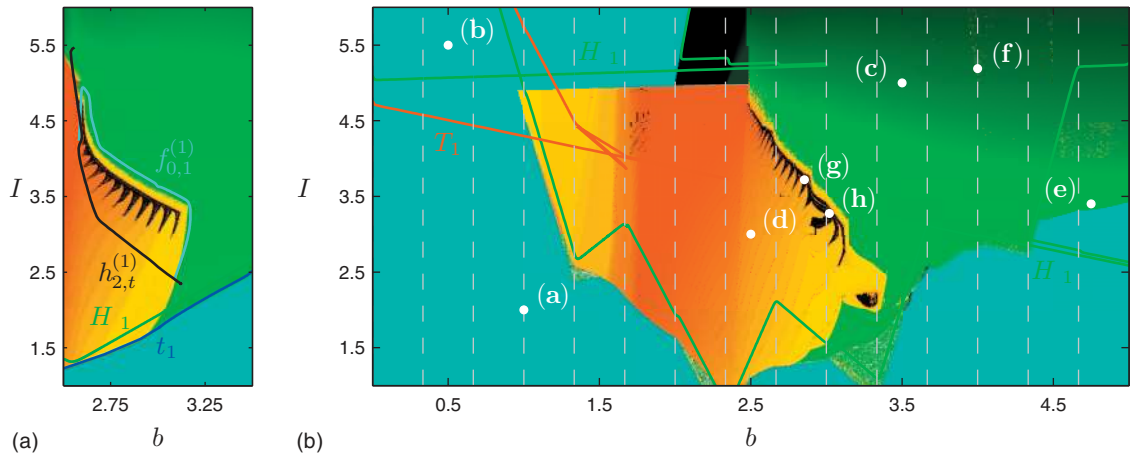

FIG. 7. (Color) Brute-force bifurcation diagrams with superimposed bifurcation curves for PWL approximations of the HR model. (a) 7×1 subdivisions of the domain $(x,b)=[-2.5,2.5]\times[2.5,3.5]$. (b) 15×15 subdivisions of the domain $(x,b)=[-4.5,5]\times[0,5]$.

in Refs. 44 and 45, this number is equal to 15 for any dimensional component.

In the latter case, on the contrary, it is convenient to reduce as much as possible the number of subdivisions. To this end, it is possible to use mixed-integer optimization procedures based on evolutionary algorithms.[26]

As can be easily seen by Eqs. (1), the nonlinearities of the model are polynomial and are confined in the first and second equations. As a consequence, to attain a PWL approximation of the model it is sufficient to approximate the nonlinear vector field with a piecewise-linear vector field defined over a two-dimensional domain.

We defined two different cost functions, thus obtaining two different PWL models. Going into details concerning the adopted optimization approaches is beyond the scope of this paper; we refer the interested reader to Ref. 26. Roughly speaking, the first model, henceforth called α model, is obtained by minimizing a cost function that depends on the weights of the basis functions only (the domain partition is fixed *a priori*) and measures the L^2 distance between the original and PWL functions all over the domain, i.e., a C^0 distance between the dynamical systems. The second model (henceforth referred to as β model), is obtained by solving (through the minimization of both a cost function and a quality factor) a mixed-integer problem that depends on both the weights of the basis functions (real variables) and the numbers of subdivisions along each domain component (integer variables). Both the cost function and the quality factor take into account some dynamical features of the system to be approximated. In particular, for the approximation of the HR model, we focused on the Hopf bifurcation curve H_1 and on the C^1 distance between the dynamical systems all over the domain. The β model provides a better tradeoff between approximation accuracy and model complexity, at the cost of a heavier optimization approach.

Figure 7 shows the brute-force bifurcation diagrams obtained by using (a) the β model; with seven subdivisions along $x\in[-2.5,3.5]$ and one along $b\in[2.5,3.5]$; and (b) the α model, by fixing 15 subdivisions along both components of the domain ($x\in[-4.5,5]$ and $b\in[0,5]$). The α model is suitable for mixed-signal circuit implementations, whereas the β model (also due to its simplicity, since the number of basis functions is $N=16$) is suitable for analog circuit implementations.

A continuation analysis requires a smoothing of the vector field.[27] In order to meet the smoothness requirements imposed by the continuation methods, we used the following smoothed version of the *absolute value* function: $g(u)=2u/\pi\arctan(au)$, where the parameter a controls the degree of smoothness. In our continuations, we fixed $a=40$, which guarantees a good tradeoff between smoothness and shape preservation of the PWL vector field. The obtained bifurcation curves are superimposed to the brute-force bifurcation diagrams.

Figure 7(a) shows the fold of cycles bifurcation curve t_1, the (subcritical) Hopf curve H_1, the flip curve $f_{0,1}^{(1)}$, and the homoclinic curve $h_{2,t}^{(1)}$. A direct comparison with Fig. 2 shows evidence that the bifurcation scenario is preserved and all the dynamical behaviors are maintained by the approximated model.

The bifurcation diagram shown in Fig. 7(b) (where the vertical lines mark the subdivisions of the domain along the b component) qualitatively matches the original model, even if, from a quantitative standpoint, the result is less accurate. This is evident also by looking at the bifurcation curve H_1. The fold of equilibria bifurcation curve T_1 is quite accurate.

In order to find a better approximation also from a quantitative standpoint, one should obtain the model parameters by minimizing the same cost function as for the β model.

Some examples of asymptotic trajectories are shown in Fig. 8, where the black (gray) trajectories are generated by the α PWL (HR) model for parameter pairs (b,I) corresponding to the dots labeled from (a) to (h) in Figs. 2(a) and 7(b). The eight parameter pairs correspond to the eight qualitatively different regions (see Sec. III A) of the original HR model. For the equilibria (light-gray dots), also the transient trajectories (starting from the gray squares) are shown. It is evident the good matching between the trajectories of the HR and α PWL models, obtained for the same parameter pairs.

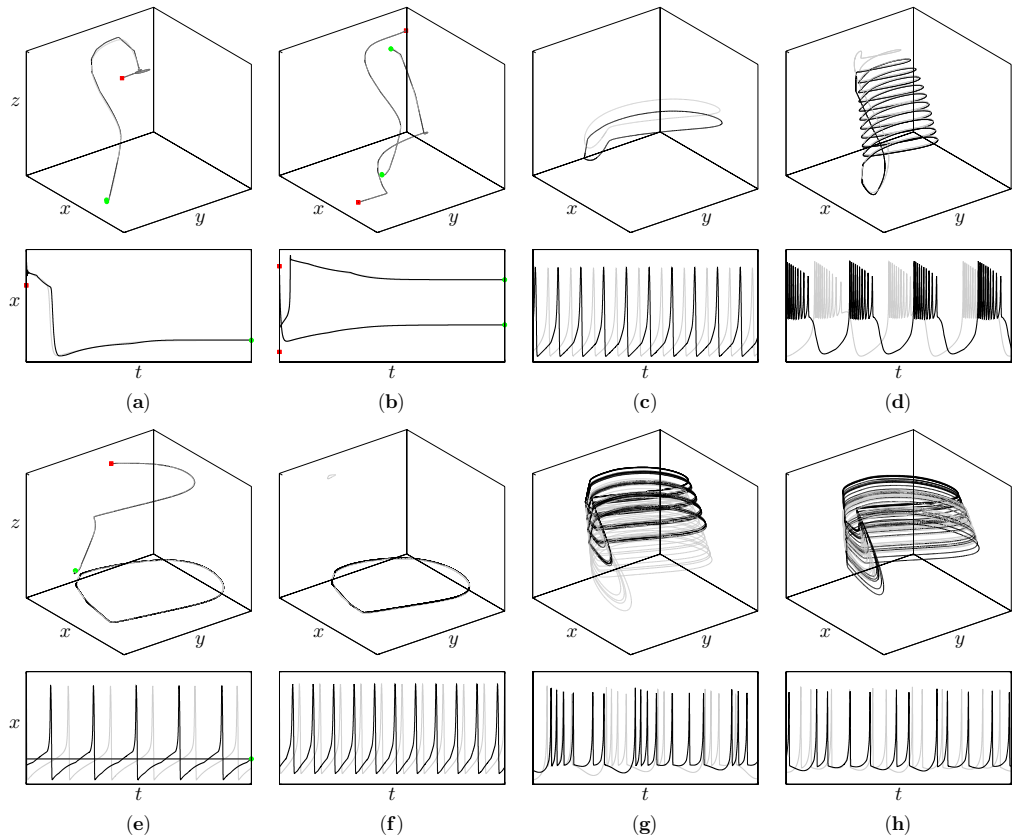

FIG. 8. (Color online) Stable invariant sets (upper panels in each pair) and time series $x(t)$ (lower panels) corresponding to points (a)–(h) in Figs. 2(a) and 7(b). Black (gray) trajectories are generated by the α PWL (HR) model. Behaviors: quiescence [(a), (b), and (e)], spiking [(c), (e), and (f)], bursting (d), irregular bursting (g), and irregular spiking (h).

This is another element that reinforces our claim that the PWL approximation can provide circuits whose dynamical behaviors are very faithful to the HR ones and can be selected by acting on two control parameters.

VI. CONCLUSIONS

This paper outlined the bifurcation structure of the HR model using a two-parameter analysis and derived a PWL approximation of the HR neuron model. Both original and approximate models have been analyzed by combining extensive simulations (exploring the parameter space) with numerical continuation methods (by using AUTO2000 and MATCONT). The use of continuation techniques in addition to extensive simulations allows us to obtain both a global picture of the bifurcation scenario and detailed information about specific bifurcation curves, e.g., the families of homoclinic bifurcation curves.

We focused on a previously reported combination of bifurcation parameters (b,I), showing that the organizing principles we found are in fact typical for the model (and not specific for this combination of parameters). Our results thus summarize and extend those previously reported in the literature and give an overview of the general organizing structure of the model, rather than focusing on certain specific features, thus providing a global picture of the bifurcation scenario to be reproduced by the PWL models. We found a good match between the dynamical behaviors exhibited by the HR model and by its PWL approximations.

The PWL approximations have been obtained by resorting to two different optimization techniques and lead to two different circuit implementations. In both cases, the results show the possibility of obtaining diversity of neural response by properly controlling the two bifurcation parameters. The next step will be the implementation (according to available techniques) of a circuit with two control parameters (b and I), allowing one to obtain qualitatively different spike-train patterns as responses to identical input currents, mimicking the natural diversity of neural response.

The general bifurcation scenario of the HR model reported in this paper can be also used as a guideline in neuronal modeling studies to fit the HR model to different electrical response patterns observed in real neurons.

In summary, the main contributions of this paper are three:

- Application of a general method of bifurcation analysis to the HR model provides a global bifurcation scenario over the parameter plane (b,I);
- the bifurcation scenario, in turn, gives concrete information about the HR model and its organizing principles, that are useful in more biophysically oriented studies;
- the obtained PWL approximations turn out to be reliable,

showing a good matching of their dynamics with respect to the HR model all over the (b,I) plane. This provides a road-map for the subsequent circuit implementation of the model and, consequently, to the use of the circuit as the elementary component of a network of neurons with different behaviors.

ACKNOWLEDGMENTS

The authors are grateful to their colleagues and friends Oscar De Feo, Federico Bizzarri, and Daniele Stellardo for valuable comments and discussions, and to the anonymous reviewers for their comments, which improved the manuscript. This work was supported by MIUR, within the PRIN framework (Project No. 2006093814), and by the University of Genoa.

[1] J. L. Hindmarsh and R. M. Rose, Nature (London) **296**, 162 (1982).
[2] J. L. Hindmarsh and R. M. Rose, Proc. R. Soc. London, Ser. B **221**, 87 (1984).
[3] R. FitzHugh, Biophys. J. **1**, 445 (1961).
[4] A. L. Hodgkin and A. F. Huxley, J. Physiol. (London) **117**, 500 (1952).
[5] A. V. M. Herz, T. Gollisch, C. K. Machens, and D. Jaeger, Science **314**, 80 (2006).
[6] E. M. Izhikevich, Int. J. Bifurcation Chaos Appl. Sci. Eng. **10**, 1171 (2000).
[7] D. Terman, SIAM J. Appl. Math. **51**, 1418 (1991).
[8] D. Terman, J. Nonlinear Sci. **2**, 135 (1992).
[9] X. J. Wang, Physica D **62**, 263 (1993).
[10] V. N. Belykh, I. V. Belykh, M. Colding-Jorgensen, and E. Mosekilde, Eur. Phys. J. E **3**, 205 (2000).
[11] J. M. González-Miranda, Chaos **13**, 845 (2003).
[12] J. M. González-Miranda, Int. J. Bifurcation Chaos Appl. Sci. Eng. **17**, 3071 (2007).
[13] G. Innocenti, A. Morelli, R. Genesio, and A. Torcini, Chaos **17**, 043128 (2007).
[14] A. Dhooge, W. Govaerts, and Yu. A. Kuznetsov, ACM Trans. Math. Softw. **29**, 141 (2003).
[15] E. J. Doedel, R. C. Paffenroth, A. R. Champneys, T. F. Fairgrieve, Yu. A. Kuznetsov, B. Sandstede, and X. Wang, Computer Science Department, Concordia University, Montreal, Quebec, Canada, 2001.
[16] A. R. Champneys, Yu. A. Kuznetsov, and B. Sandstede, Int. J. Bifurcation Chaos Appl. Sci. Eng. **6**, 867 (1996).
[17] A. Champneys and Y. Kuznetsov, Int. J. Bifurcation Chaos Appl. Sci. Eng. **4**, 785 (1994).
[18] D. Stellardo, F. Bizzarri, M. Storace, and O. De Feo, Chaos **17**, 043108 (2007).
[19] E. de Lange, "Neuron models of the generic bifurcation type: Network analysis and data modeling," Ph.D. thesis, EPFL, 2006.
[20] E. de Lange and M. Hasler, "Predicting single spikes and spike patterns with the Hindmarsh–Rose model," Biol. Cybern. (submitted).
[21] P. Julián, A. Desages, and O. Agamennoni, IEEE Trans. Circuits Syst., I: Fundam. Theory Appl. **46**, 463 (1999).
[22] P. Julián, A. Desages, and B. D'Amico, IEEE Trans. Circuits Syst., I: Fundam. Theory Appl. **47**, 702 (2000).
[23] M. Storace, L. Repetto, and M. Parodi, Int. J. Circuit Theory Appl. **31**, 277 (2003).
[24] M. Storace and M. Parodi, Int. J. Circuit Theory Appl. **33**, 147 (2005).
[25] M. Parodi, M. Storace, and P. Julián, Int. J. Circuit Theory Appl. **33**, 307 (2005).
[26] D. Linaro, F. Bizzarri, and M. Storace, "Piecewise-linear approximation of the Hindmarsh–Rose neuron model," J. Phys.: Conf. Ser. (in press).
[27] M. Storace and O. De Feo, IEEE Trans. Circuits Syst., I: Regul. Pap. **51**, 830 (2004).
[28] M. Storace and F. Bizzarri, IEEE Trans. Circuits Syst., I: Regul. Pap. **54**, 620 (2007).
[29] M. Denker, A. Szücs, R. D. Pinto, H. D. I. Abarbanel, and A. I. Selverston, IEEE Trans. Biomed. Eng. **52**, 792 (2005).
[30] Y. J. Lee, J. Lee, K. K. Kim, Y. B. Kim, and J. Ayers, Neurocomputing **71**, 284 (2007).
[31] B. Krauskopf, K. Schneider, J. Sieber, S. Wieczorek, and M. Wolfrum, Opt. Commun. **215**, 367 (2003).
[32] M. Kisaka, H. Kokubu, and H. Oka, J. Dyn. Differ. Equ. **5**, 305 (1993).
[33] A. J. Homburg and B. Krauskopf, J. Dyn. Differ. Equ. **12**, 807 (2000).
[34] L. Belyakov, Matematiecheskie Zametki **15**, 336 (1974).
[35] L. Belyakov, Matematiecheskie Zametki **28**, 910 (1980).
[36] L. Belyakov, Matematiecheskie Zametki **36**, 838 (1984).
[37] P. Glendinning and C. Sparrow, J. Stat. Phys. **35**, 645 (1984).
[38] B. Sandstede, "Verzweigungstheorie homokliner Verdopplungen," Ph.D. thesis, University of Stuttgart, 1993.
[39] V. Vapnik, *Estimation of Dependencies Based on Empirical Data* (Springer, Berlin, 1992).
[40] T. Poggio and F. Girosi, Proc. IEEE **78**, 1481 (1990).
[41] G. Wahba, *Spline Models for Observational Data*, Series in Applied Mathematics (SIAM, New York, 1990), Vol. 59.
[42] M. S. Floater, E. G. Quak, and M. Reimers, J. Comput. Appl. Math. **119**, 185 (2000).
[43] T. Takagi and M. Sugeno, IEEE Trans. Syst. Man Cybern. **15**, 116 (1985).
[44] M. Di Federico, P. Julián, T. Poggi, and M. Storace, in Proceedings of the 2007 IEEE International Symposium on Circuits and Systems (ISCAS'07), New Orleans, Louisiana, 2007, pp. 685–688.
[45] A. Boggiano, S. Delfitto, T. Poggi, and M. Storace, in Proceedings of the European Conference on Circuit Theory and Design (ECCTD'07), Seville, Spain, 2007, pp. 874–877.